# Supplementary file

# Investigating rock properties and fracture propagation pattern during supercritical

### CO<sub>2</sub> pre-fracturing in conglomerate reservoir

Hang Zhou<sup>1, 3</sup>, Tingwei Yan<sup>2</sup>, Japan Trivedi<sup>3</sup>, Bo Wang<sup>2, \*</sup>, Fujian Zhou<sup>1</sup>

<sup>1</sup> State Key Laboratory of Petroleum Resources and Engineering, China University of Petroleum, Beijing 102249, P. R. China

<sup>2</sup> College of Petroleum, China University of Petroleum-Beijing at Karamay, Karamay 834000, P. R. China

<sup>3</sup> Faculty of Engineering-Civil and Environmental Engineering, University of Alberta, Edmonton, Alberta T6G 2R3, Canada

E-mail address: 2023311224@student.cup.edu.cn (H. Zhou); weitingyan2000@163.com (T. Yan); jtrivedi@ualberta.ca (J.

Trivedi); wangbo@cupk.edu.cn (B. Wang); zhoufj@cup.edu.cn (F. Zhou).

\* Corresponding author (ORCID: 0000-0002-9898-5551 (B. Wang))

Zhou, H., Yan T., Trivedi, J., Wang, B., Zhou, F. Investigating rock properties and fracture propagation pattern during supercritical CO<sub>2</sub> pre-fracturing in conglomerate reservoir. Advances in Geo-Energy Research, 2025, 17(2): 95-106.

The link to this file is: https://doi.org/10.46690/ager.2025.08.02

## Appendix A

XRD analyzed the mineral composition of the matrix and cement in samples. As shown in Table A1, the clay mineral content in the matrix and cement of Upper Wuerhe Formation conglomerates exceeds 30%, predominantly with clay cementation. In contrast, the Baikouquan Formation conglomerates exhibit lower clay mineral contents in their matrix and cement, predominantly with calcite cementation.

Table A1. Results of mineral fraction.

NO.	Horizon	Mineral fraction					
110.		Clay	Quartz	Plagioclase	Calcite	Pyrite	K-feldspar
C1	P3w	32.5	41.6	23	/	/	2.9
C2	P3w	40.2	44.8	11.9	/	/	3.1
C3	P3w	29.3	49.1	18.2	/	/	2.4
C4	P3w	35.4	41.8	19.6	/	/	3.2
C5	P3w	45.3	31.7	17.1	/	/	5.9
C6	T1b	22.5	35.8	35.4	2.1	4.2	/

Based on high-precision CT scanning of core samples, 3D digital cores of conglomerates were reconstructed to characterize the internal structural features of conglomerate cores (gravel content and particle size parameters). Gravel in conglomerates was extracted through threshold segmentation, gravel identification, smoothing, and integral calculation to quantify gravel content and particle size distribution (Orrú et al., 2014; Soloy et al., 2020), as shown in Fig. A2. The gravel content exceeds 50%, with gravel sizes ranging between 8 and 14 mm in particle-supported conglomerates (C1 and C2). The gravel content exceeds 35%, with gravel sizes ranging between 2 and 14 mm in multi-size particle-supported conglomerates (C3, C4, and C6). The gravel content is below 30%, with gravel sizes ranging between 2 and 14 mm in matrix-particle-supported conglomerates (C5).

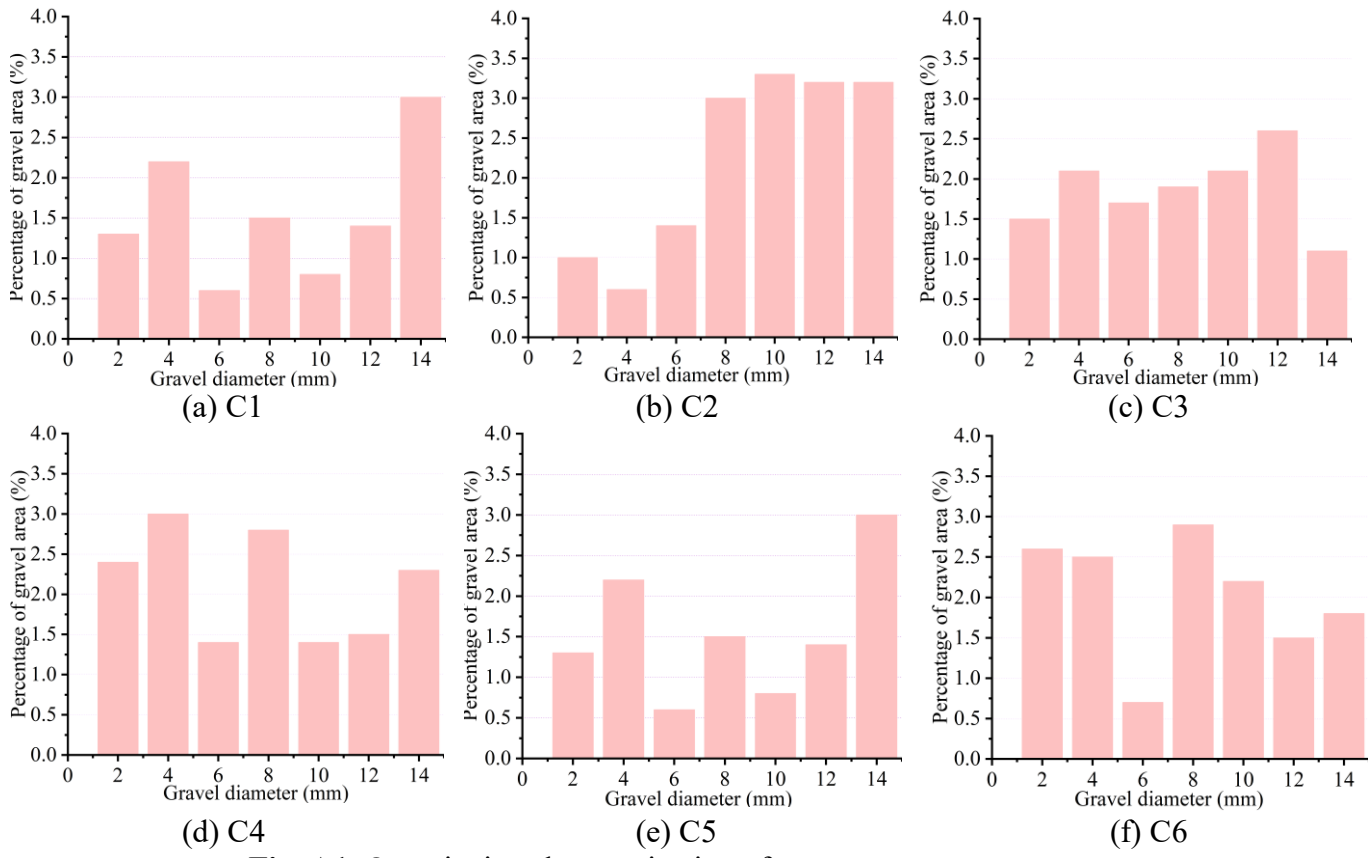


Fig. A1. Quantitative characterization of core component parameters.

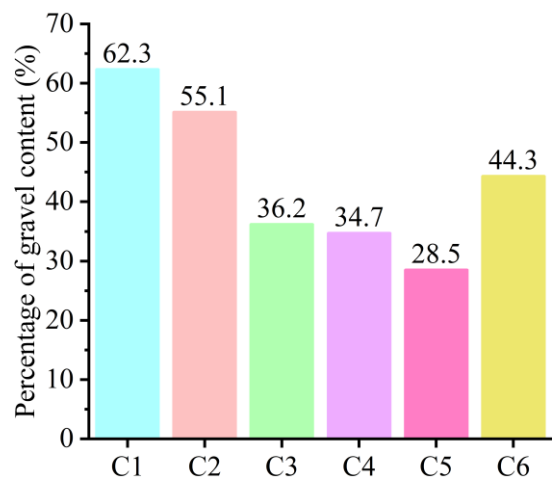
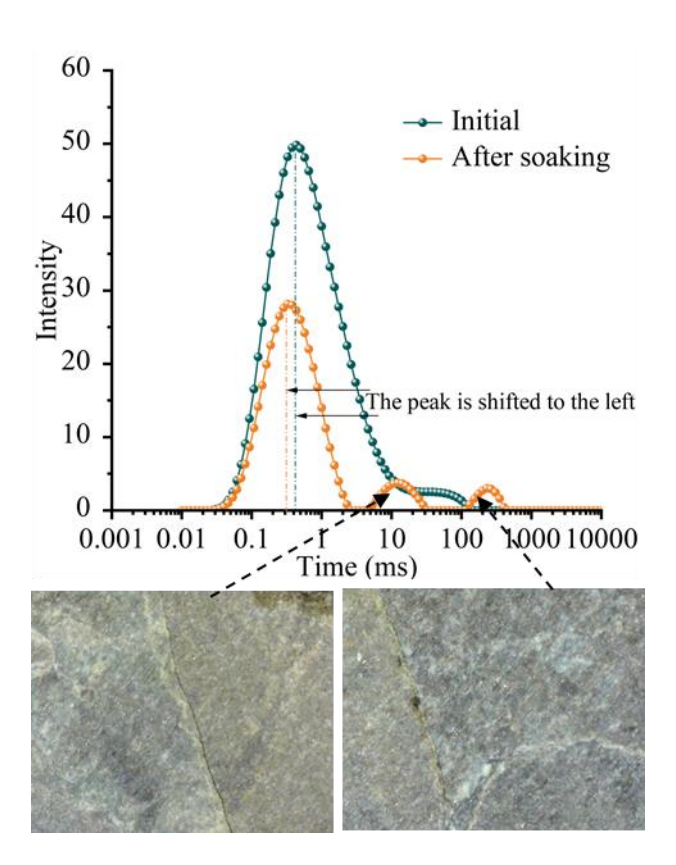


Fig. A2. Percentage of gravel content.

#### Appendix B

The surface morphology and NMR T<sub>2</sub> spectra of various conglomerate types before and after CO<sub>2</sub> soaking are illustrated in Figs. B1-B3. Observations of the core surfaces before and after soaking indicate that intense CO<sub>2</sub> diffusion induces dissolution of the cementation interfaces among gravels (C1-2), the matrix in fine-grained, gravel-rich zones (C4-2, C5-2), and the matrix in C6-2. This process gives rise to the formation of dissolution pores and microfractures. Simultaneously, the NMR T<sub>2</sub> spectra of the cores reveal that several small new peaks emerge on the right side of the spectrum after CO<sub>2</sub> soaking, indicating the in-situ formation of numerous dissolution pores and microfractures within the core. These dissolution features are principal channels for fracturing fluid leak-off during subsequent hydraulic fracturing. The injected fracturing fluid can rapidly migrate through these preferential flow pathways to deeper rock strata, significantly enhancing the penetration depth of artificial fractures. This further demonstrates that the fractures formed by dissolution during soaking dictate subsequent hydraulic fractures' location and penetration depth.



**Fig. B1.** Test results of C1-2 samples before and after soaking.

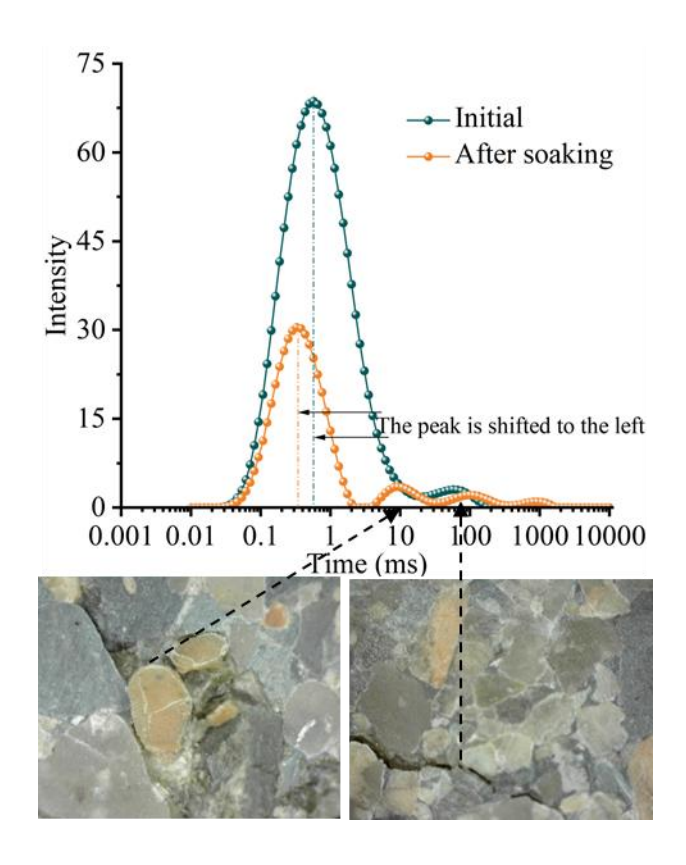


Fig. B2. Test results of C5-2 samples before and after soaking.

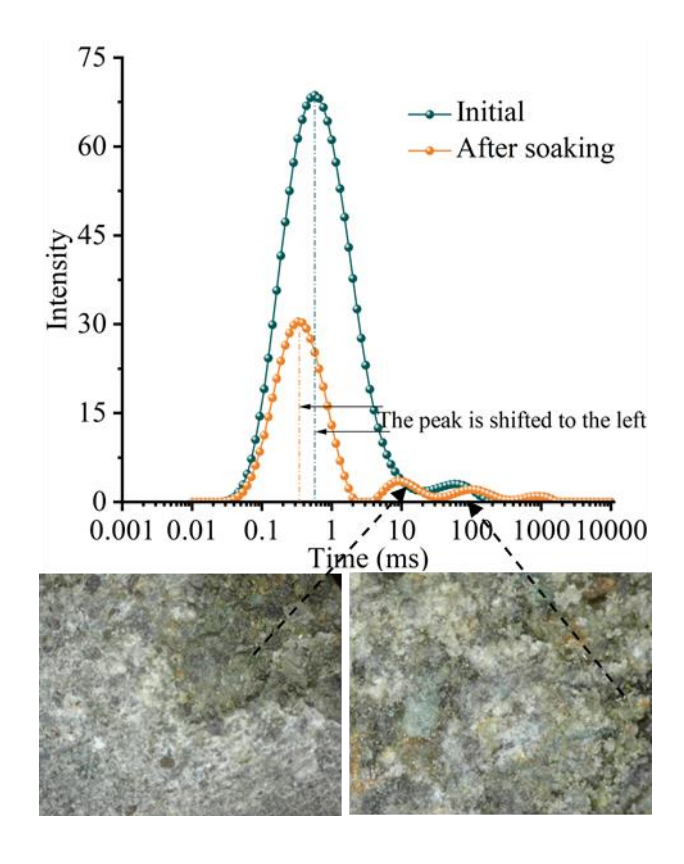


Fig. B3. Test results of C6-2 samples before and after soaking.